ISSN 0973-3450 (Print)
JUC Vol. 22(4), 77- 91 (2026). Periodicity 2-Monthly
ISSN 2319-8036 (Online)

JOURNAL OF ULTRA CHEMISTRY
An International Open Free Access Peer Reviewed Research Journal of Chemical Sciences and Chemical Engineering
website:- www.journalofchemistry.org
Estd. 2005

Novel Mixed-Ligand Ruthenium(III) Complexes Incorporating 2-Aminomethylbenzimidazole: Synthesis, Structural Characterization, and Biological Evaluation

KIRTI VARDHAN GAUTAM[1*], RAKESH KUMAR RANJAN[2], SHEO SHANKAR KUMAR[3] and UTKARSH DEEPANKAR[4]

[1]Department of Chemistry, S.S.V. College, Kahalgaon, Tilka Manjhi Bhagalpur University, Bhagalpur-813203, Bihar (INDIA)
[2]Department of Chemistry, College of Commerce, Arts & Science, Patliputra University, Patna-800020, Bihar (INDIA)
[3]Department of Chemistry, College of Commerce, Arts & Science, Patliputra University, Patna-800020, Bihar (INDIA)
[4]Department of Civil Engineering, Indian Institute of Technology (Indian School of Mines), Dhanbad-826004, Jharkhand (INDIA)
* Corresponding author: Kirti Vardhan Gautam (drkvgautam@gmail.com)

DOI : http://dx.doi.org/10.22147/juc/220403

Acceptance Date 13th October 2026 **Online Publication Date 27th October 2026**

Abstract

A series of three new halide-free ruthenium (III) complexes was synthesized using 2-aminomethylbenzimidazole as the principal chelating ligand in combination with different auxiliary ligand systems. Their compositions and coordination behavior were investigated through elemental analysis, conductivity measurements, UV-Visible spectroscopy, magnetic susceptibility studies, FT-IR spectroscopy, and low-temperature EPR spectroscopy. The overall experimental findings support the formation of mononuclear Ru(III) complexes exhibiting 1:1 electrolyte behavior and a low-spin d^5 Ru(III) center adopting a distorted octahedral coordination geometry. The interactions of the synthesized complexes with biological macromolecules were examined by employing absorption and fluorescence titration methods. The findings obtained from DNA-binding experiments showed that the complex with the aromatic diimine ligand presented the highest affinity

This is an open access article under the CC BY-NC-SA license (https://creativecommons.org/licenses/by-nc-sa/4.0/)

toward calf thymus DNA, in agreement with a partial intercalative mode of association. Fluorescence quenching studies with Bovine Serum Albumin (BSA) indicated the formation of stable protein–complex adducts predominantly through a static quenching mechanism. The antiproliferative activities of the complexes were examined against HeLa and MCF-7 cell lines, revealing a concentration-dependent inhibition of cell growth. These observations underline the importance of ligand architecture in controlling biological activity, making these complexes attractive candidates for targeted metallodrug design.

Key words : Ruthenium(III) complexes, 2-aminomethylbenzimidazole, halide-free coordination compounds, DNA binding, BSA interaction.

Introduction

The discovery of cisplatin and its eventual clinical success made metal-based therapeutics a major component of modern cancer therapy. Platinum containing drugs are used extensively but have several inherent limitations, such as systemic toxicity, acquired resistance, and poor tumor selectivity, which restrict their long term therapeutic efficacy. Consequently, considerable research efforts have been devoted to the development of non-platinum metallodrugs to overcome these shortcomings. Ru complexes have attracted considerable demonstrate potential as alternatives associated with their versatile coordination chemistry, accessible redox chemistry, and capacity to utilize biological metal- transport pathways mediated by interactions with serum proteins, including transferrin and albumin[1,2].

Notably, octahedral Ru(III) complexes possess a unique therapeutic advantage in that they may act as prodrugs, undergoing reductive activation under physiological or tumour-associated conditions to generate biologically active Ru(II) species, thereby contributing to enhanced selectivity and therapeutic performance. Prototypical Ru(III) coordination entities such as NAMI-A and KP1019 have succeeded such a therapeutic approach to advanced clinical trials, thus highlighting the clinical viability of paramagnetic low-spin d^5 Ru systems[3-5].

The electronic properties and steric characteristics of both the primary chelating and ancillary ligands play a fundamental role in determining biodistribution, aquation kinetics, and macromolecular affinity of the Ru complexes. Benzimidazole and its functional derivatives such as, 2-aminomethylbenzimidazole, are a privileged class of nitrogen-donor heterocycles. The fused bicyclic benzimidazole pharmacophore offers increased lipophilicity, interaction with a planar π-system, and hydrogen bonding potential. Coordination of 2-aminomethylbenzimidazole to a Ru(III) center leads to the establishment of a stable five-membered chelate arrangement. Exposure of functional amine moieties that can involve in non-covalent interactions with biomolecular targets of interest such as genomic DNA and serum proteins[6-8].

Classical chloro-bridged Ru(III) complexes are promising therapeutic agents but suffer from rapid aquation in aqueous physiological buffers, which can result in premature ligand dissociation, non-specific protein binding, and off-target side effects. A versatile approach to overcome these systemic liabilities is the replacement of coordination-sphere halides by robust pseudohalides such as azide and thiocyanate or chelating dicarboxylates such as oxalate. This enables modulation of the electronic density at the metal core, stabilization of the trivalent oxidation state, and fine-tuning of lipophilicity. Furthermore, a synergistic advantage is obtained using sterically demanding diphosphines,

like 1,2-bis(diphenylphosphino) ethane, monophosphines, or extended aromatic diimines such as 5,6-dimethyl-1,10-phenanthroline. Extended aromatic frameworks greatly enhance the non-covalent intercalation between DNA base pairs and the static quenching with serum albumins. Hydrophobic phosphine and methyl-phenanthroline co-ligands promote cellular transmembrane transport.[9–11]

In view of the above, we report the design, synthesis, complete spectral profiling, and in vitro biological evaluation of three novel, halide-free mixed-ligand Ru (III) complexes incorporating 2-aminomethylbenzimidazole together with azide, thiocyanate, or oxalate co-ligands. They are $[Ru(N_3)_2(dppe)(AMBzl)]\ NO_3$ —Complex 1, $[Ru(ox)(dmphen)(AMBzl)]\ PF_6$ — Complex 2, and $[Ru(NCS)_2(PPh_3)_2(AMBzl)]\ NO_3$ —Complex 3**.** The present study furnishes a complete overview concerning the effect of strategic integration of pseudohalide and dicarboxylate ligands with phosphine and diimine auxiliaries on spectroscopic signatures, magnetic properties, DNA and serum albumin binding affinities, and cytotoxic potency against human cervical and breast carcinoma cell lines.[12–20]

2 Materials and Experimental Methods

2.1 Reagents & Materials

High-purity Ru(III) chloride hydrate ($RuCl_3.xH_2O$), 2-aminomethylbenzimidazole dihydrochloride (AMBzl·HCl), 1,2-bis(diphenyl-phosphino) ethane (dppe), 5,6-dimethyl-1,10-phenanthroline (dmphen), triphenylphosphine (PPh_3), sodium azide (NaN_3), potassium thiocyanate (KSCN), sodium oxalate ($Na_2C_2O_4$), ammonium hexafluorophosphate (NH_4PF_6), and silver nitrate ($AgNO_3$) were purchased from commercial sources, such as Sigma Aldrich and Merck. All reagents employed in the study were of analytical grade, with a reported purity exceeding 98%. Highly purified CT-DNA, BSA, and ethidium bromide (EtBr) were procured from Sigma Aldrich and used for the biological interaction studies. Organic solvents (spectroscopic and analytical grades) such as acetonitrile, methanol, dimethylformamide (DMF), ethanol, dimethyl sulfoxide (DMSO), and diethyl ether were dried with appropriate desiccant agents and freshly distilled under a nitrogen atmosphere before use in synthetic procedures.

2.2 Instrumentation and Measurement Techniques :

Carbon, hydrogen, and nitrogen contents were quantified using a Perkin-Elmer 2400 Series II CHNS/O elemental analyzer. The electrolytic behavior was determined by measurement of the molar conductivity of the millimolar solution concentrations (10^{-3} M) in anhydrous DMF at 25 ± 1°C using a Systronics Conductivity Bridge 304 equipped with a glass conductivity cell. Solid-state magnetic susceptibility measurements were recorded at room temperature (298 K) using the Gouy balance method, with mercury tetrathiocyanatocobaltate(II), $Hg[Co(NCS)_4]$, serving as the calibration standard. Diamagnetic corrections were applied using Pascal's constants. FT-IR spectra were acquired using a Thermo Nicolet iS50 spectrophotometer over the 4000–400 cm^{-1} range, with potassium bromide (KBr) pelletized samples prepared for analysis. The electronic absorption spectra were acquired across the 200–800 nm wavelength range in DMF solutions at ambient temperature using a Shimadzu UV-2600 a double-beam spectrophotometer equipped with matched quartz cuvettes having a 1.0 cm optical path length. Low-temperature X-band EPR spectra were determined at 77 K in frozen DMF matrices using a Bruker EMX spectrometer. The measurements were performed at a nominal

microwave frequency of 9.45 GHz with 100 kHz magnetic-field modulation.

2.3 Synthesis of Ru^{III} Complexes

2.3.1 Synthesis of $[Ru(N_3)_2(dppe)(AMBzl)]NO_3$ (Complex 1)

Bis(azido)(1,2-bis(diphenylphosphino) ethane)(2-aminomethylbenzimidazole) ruthenium(III) Nitrate : Ru(III) chloride hydrate (0.207 g, 1.0 mmol) was added as a solution in hot methanol (20 mL). A 10 mL dichloromethane solution containing 1,2-bis(diphenylphosphino) ethane (dppe, 0.398 g, 1.0 mmol) was subsequently added dropwise to the prepared solution, and the reaction mixture was subjected to reflux conditions for 1 h. Then, aqueous solutions of 2-aminomethylbenzimidazole (AMBzl, 0.147 g, 1.0 mmol) and sodium azide (NaN_3, 0.130 g, 2.0 mmol) in minimal amounts of water were added. The resulting mixture was refluxed for an additional 4 h under an inert atmosphere of nitrogen. Silver nitrate ($AgNO_3$, 0.170 g, 1.0 mmol) was introduced to precipitate the unbound chloride ions as AgCl, which was filtered off. The resulting residue was concentrated under reduced pressure and subsequently precipitated using diethyl ether (ice-cold) to give a reddish-brown solid. The precipitated solid was filtered, successively washed with cold ethanol and diethyl ether, and dried under vacuum over phosphorus pentoxide (P_4O_{10}). The proposed structure for Complex 1 is illustrated in Figure 1, which supports our theoretical analysis.

Yield: 72%. Color: Reddish brown. Decomposition temperature: >245°C. Analytical Calculation for $C_{34}H_{33}N_{10}O_3P_2Ru$ (%): Calcd.: C, 51.00; H, 4.15; N, 17.49 Found: C 50.84, H 4.08, N 17.32.

2.3.2 Synthesis of $[Ru(ox)(dmphen)(AMBzl)]PF_6$ (Complex 2)

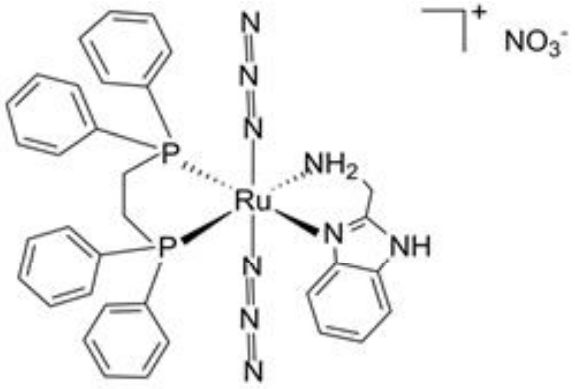


Figure 1 The proposed structure of $[Ru(N_3)_2(dppe)(AMBzl)]NO_3$ complex.

(Oxalato)(5,6-dimethyl-1,10-phenanthroline) (2-aminomethylbenzimidazole)ruthenium(III) Hexafluorophosphate : A solution of 5,6-dimethyl-1,10-phenanthroline (dmphen, 0.208 g, 1.0 mmol) in ethanol (20 mL) was magnetically stirred, followed by the subsequent addition of Ru(III) chloride hydrate (0.207 g, 1.0 mmol), and the resulting mixture was maintained at 60 °C with continuous stirring for 45 min. Following the above step, Sodium oxalate ($Na_2C_2O_4$, 0.134 g, 1.0 mmol) dissolved in warm water (5 mL) and 2-aminomethylbenzimidazole (AMBzl, 0.147 g, 1.0 mmol) were introduced into the flask. The reaction was permitted to proceed under reflux for 5 h, giving a deep violet color. After allowing the reaction mixture to cool to room temperature, an aqueous solution of ammonium hexafluoro-phosphate (NH_4PF_6, 0.195 g, 1.2 mmol) was introduced and added dropwise with stirring. A deep purple solid immediately precipitated. The precipitated crude product was filtered and successively washed with ice-cold distilled water and ethanol, and dried under vacuum. The proposed structure for Complex 2 is illustrated in Figure 2, which supports our theoretical analysis.

Yield: *78%*. Color: Deep purple. Decomposition Temperature: >260°C Analytical Calculation for

$C_{24}H_{21}F_6N_5O_4PRu$: Cald: C, 41.81; H, 3.07; N, 10.16. Found C, 41.65; H, 2.98; N, 10.05.

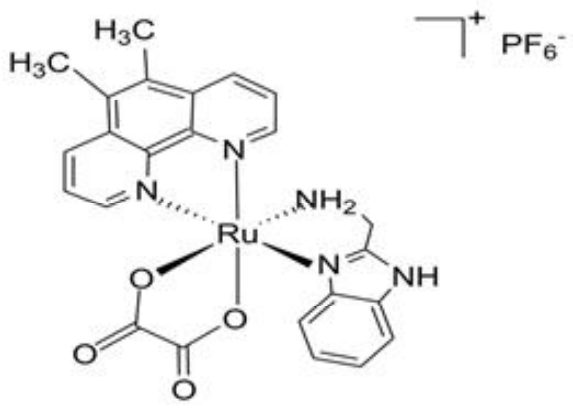


Figure 2. The proposed structure of [Ru(ox)(dmphen)(AMBzl)] PF_6 complex.

2.3.3 Synthesis of $[Ru(NCS)_2(PPh_3)_2$ (AMBzl)] NO_3 (Complex 3)

Bis(isothiocyanato)bis(triphenylphosphine)(2-aminomethylbenzimidazole)ruthenium(III) Nitrate : A mixture of Ru(III) chloride hydrate (0.207 g, 1.0 mmol) and triphenylphosphine (PPh_3, 0.524 g, 2.0 mmol) in ethanol (25 mL) was heated under thermal reflux for 1 h. Potassium thiocyanate (KSCN, 0.194 g, 2.0 mmol) together with 2-aminomethylbenzimidazole (AMBzl, 0.147 g, 1.0 mmol) were then added to the reaction vessel and heating under reflux was further continued for 6 h. Anion metathesis was performed by the addition of silver nitrate ($AgNO_3$, 0.170 g, 1.0 mmol) to precipitate the free chloride as silver chloride. The reaction mixture was filtered while hot, and the resulting filtrate was concentrated to approximately one-third of the original volume and kept undisturbed at 4 °C overnight. The resulting dark brown microcrystals were obtained through filtration, purified by successive washing with cold ethanol and diethyl ether followed by drying under vacuo. The proposed structure for Complex 3 is illustrated in Figure 3, which supports our theoretical analysis.

Yield**:** 68% Color: Dark brown. Decomposition Temperature: > 238°C. Analytical Calculation for $C_{46}H_{39}N_6O_3P_2S_2Ru$ (%): Cald: C, 57.61; H, 4.10; N, 8.76. Found: C, 57.42; H, 4.01; N, 8.62.

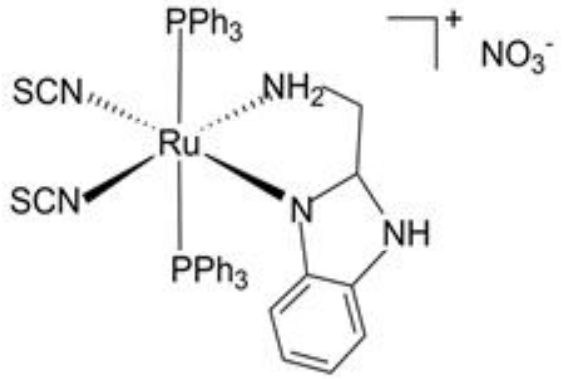


Figure 3 Proposed molecular structure of $[Ru(NCS)_2(PPh_3)_2(AMBzl)]$ NO_3

2.4 Methodologies for DNA/BSA Binding Interactions and Antiproliferative Evaluation

2.4.1 Spectrophotometric DNA Binding Titration Protocols

The affinity of the synthesized complexes (1-3) toward CT-DNA was evaluated by electronic absorption titrations in the Tris-HCl buffer consisting of Tris-HCl and sodium chloride at physiological pH at room temperature. The purity of the nucleic acid stock solution was confirmed by calculating the ratio of ultraviolet absorbance at 260 nm and 280 nm, which gave a range suitable for binding measurements. Titrations were performed using a constant concentration of the Ru complex and upon successive addition of increasing volumes of the DNA stock solution. All reaction mixtures were allowed an equilibration period prior to spectral acquisition.

The quantitative binding parameters and intrinsic binding constants were then calculated from the absorption data using the established mathematical relationships reported in the literature.[21–23]

2.4.2 BSA Fluorescence Quenching and Binding Assay Protocols

Binding interactions of the synthesized ruthenium complexes with BSA in phosphate buffer saline at physiological pH was characterized through fluorescence spectroscopy. During the measurements the BSA concentration was constant and emission spectra were recorded in the characteristic UV-visible region after excitation of the tryptophan residues of the protein. Stepwise addition of the individual complex solutions to the protein sample was performed, and then the fluorescence titration experiments were undertaken. The characteristic fluorescence intensity of BSA was decreased steadily with successive increases in the complex concentration employed, which indicated the interaction between protein and complex. The corresponding quenching behavior was analyzed by using the established spectroscopic models to quantify the Stern–Volmer quenching constant (K_{SV}), bimolecular quenching constant (K_q), association constant (K_b), and binding-site number (n).[24,25]

2.4.3 In Vitro Antiproliferative and MTT Cytotoxicity Assays

The antiproliferative potential of Complexes (1-3) was screened on cervical and breast carcinoma cell lines of human origin by the conventional colorimetric tetrazolium-based cell viability assay[26,33,36]. Cells were seeded in microtiter plates, grown in modified Eagle medium containing fetal bovine serum (FBS), followed by maintaining in a temperature-controlled incubator containing carbon dioxide. The cell cultures were treated with serially diluted concentrations of the test compounds for a defined incubation period of exposure after initial cell attachment. Cisplatin was analyzed in parallel as a positive comparative standard under the same conditions. The optical density was measured at the absorption wavelength of the target on a microplate reader. The dose-response profiles were generated to determine the concentration that resulted in 50 percent inhibition of cellular proliferation.[26–27]

3 Results and Discussion

3.1 Physicochemical Characterization and Molar Conductance

The synthesized mononuclear Ru(III) complexes (1–3) were obtained as air-stable solids at ambient laboratory conditions. All three compounds were very soluble showed good solubility in polar coordinating solvents, including N,N-dimethylformamide (DMF) and dimethyl sulfoxide (DMSO), moderately soluble in acetonitrile, and insoluble in non-polar media such as diethyl ether and n-hexane. The physical characteristics, yield and thermal stability data for all complexes are summarized in Table-1. Molar conductance (Λ_m) measurements were carried out using 10^{-3} M solutions in DMF at 25 °C to assess electrolytic behavior. The value obtained for Complex 1 was 78 Ω^{-1} cm^2 mol^{-1}, for Complex 2 was 68 Ω^{-1} cm^2 mol^{-1}, and for Complex 3 was 72 Ω^{-1} cm^2 mol^{-1} (Table-1). The values are in the range of 60 - 90 Ω^{-1} cm^2 mol^{-1}, which are typical for 1:1 electrolyte in DMF and imply that the nitrate (NO_3^-) and hexafluorophosphate (PF_6^-) ions are located in the outer coordination sphere.[28–30]

3.2 Magnetic Susceptibility and EPR Spectral Analysis

The solid-state magnetic susceptibility and frozen-state EPR spectral parameters (77 K) for

Table 1. Physical Characteristics and Molar Conductance Data

Complex	Color	Yield (%)	Decomp. Temp (°C)	Λ_m ($\Omega^{-1}cm^2mol^{-1}$)	Electrolytic Nature
Complex 1	Reddish-Brown	72	> 245	78	1:1 Electrolyte
Complex 2	Deep Purple	78	> 260	68	1:1 Electrolyte
Complex 3	Dark Brown	68	> 238	72	1:1 Electrolyte

Complexes 1–3 are summarized in Table 2. The solid state magnetic susceptibility measurements obtained for Complexes 1–3 at room temperature (298 K) gave effective magnetic moment (μ_{eff}) values of 1.84 B.M., 1.81 B.M. and 1.88 B.M. in the order listed (Table 2). The observed values marginally exceed the theoretical spin-only value of 1.73 B.M. for one unpaired electron (S = 1/2), confirming a low-spin t_{2g}^5 electronic configuration for mononuclear Ru(III)centers. The slight orbital contribution to the magnetic moment arises from spin-orbit coupling ($\lambda \approx$ -800 to -1000 cm^{-1}) characteristic of heavy 4d transition elements.[31–32]

X-band EPR spectral measurements were performed at 77 K in frozen DMF solutions to determine the coordination geometry around the Ru core. The three complexes show well-resolved anisotropic EPR spectra with three different g-values (g_1, g_2, g_3), which is in agreement with a distorted octahedral stereochemistry (Table 2).

The large separation of g_1 (g_x) and g_3 (g_z) shows the strong axial and rhombic ligand field splitting. The anisotropy parameter was calculated as $\Delta_g = 0.49$ for Complex 1 and 3 and $\Delta_g = 0.48$ for Complex 2. The observed anisotropy for Complex 2 is assigned to the rigid and planar 5,6-dimethyl-1,10-phenanthroline (dmphen) and chelating oxalate (ox^{-2}) ligands, which cause a large structural strain on the metal center.[33–34]

Table 2 Solid-State Magnetic Susceptibility and Frozen-State EPR Spectral Parameters (77 K)

Complex	$\chi_m \times 10^{-6}$ ($cm^3\ mol^{-1}$)	$\chi_A \times 10^{-6}$ ($cm^3\ mol^{-1}$)	μ_{eff} (B.M.)	g_1 (g_x)	g_2 (g_y)	g_3 (g_z)	⟨g⟩	Δg ($g_1 - g^3$)
Complex 1	1240	1420	1.84	2.38	2.16	1.89	2.15	0.49
Complex 2	1180	1380	1.81	2.42	2.21	1.94	2.20	0.48
Complex 3	1290	1480	1.88	2.40	2.18	1.91	2.17	0.49

3.3 FT-IR Vibrational Spectroscopy

The Fourier-Transform Infrared spectra of Complexes (1–3) in KBr pellets (4000–400 cm^{-1}) provide direct structural information on the coordination modes of 2-aminomethylbenzimidazole (AMBzl), secondary co-ligands (dppe, dmphen, PPh_3), pseudohalides (N_3^-, NCS^-), dicarboxylate (ox^{2-}), and outer-sphere counter ions (NO_3^-, PF_6^-).[35,36]

The primary amine -NH_2 asymmetric and symmetric stretching modes are found at 3380 cm^{-1} and 3250 cm^{-1} in the spectrum of the uncomplexed AMBzl ligand. Across Complexes 1–3, these bands are bathochromically shifted to 3210–3120 cm^{-1} ($\Delta\nu \approx$130–170 cm^{-1}) upon complexation, confirming coordination of the

primary aliphatic amino nitrogen atom (N_{amine}) to the Ru(III) ion. Furthermore, the azomethine C=N vibration of the benzimidazole core at 1620 cm^{-1} in free AMBzl is displaced toward lower frequencies (1575–1585 cm^{-1}), confirming secondary coordination via the tertiary imidazole nitrogen atom ($N_{pyridine}$).[37,38]

For Complex 1, a very strong and sharp absorption band observed at 2045 cm^{-1} is designated as the asymmetric azide stretch ν_{as} (N_3^-), which is characteristic of terminal N-bonded azido ligands. The coordination of 1,2-bis(diphenylphosphino) ethane (dppe) is supported by the appearance of characteristic aromatic phosphine bands at 1098 cm^{-1} (ν(P–Ar)) and 1435 cm^{-1} (ν(C=C)).[39]

In Complex 2, the coordinated oxalate (ox^{2-}) moiety exhibits intense bands at 1685 cm^{-1} (ν_{as}(C=O)) and 1390 cm^{-1} (ν_S(C–O)). The large frequency difference ($\Delta\nu = \nu_{as} - \nu_S = 295$ cm^{-1}) is characteristic of symmetric O,O'-bidentate chelation to the central Ru metal. The bands of 5,6-dimethyl-1,10-phenanthroline (dmphen) at 1515 cm^{-1} (ν(C=N)) and 825 cm^{-1} (δ (C–H)) are clearly observed.[40]

For Complex 3, a sharp intense absorption at 2085 cm^{-1} assigned to ν(C≡N) and a weaker ν(C–S) mode at 820 cm^{-1} confirm the coordination involving the nitrogen donor atom of the thiocyanate ligand (Ru-NCS, isothiocyanato coordination). The triphenylphosphine (PPh_3) coordination is reflected by characteristic vibrations at 1438 cm^{-1} (ν(P–Cphenyl)) and 695cm^{-1} (γ(C–H)$_{phenyl}$).[41]

The presence of uncoordinated ionic counter ions in the outer coordination sphere is unequivocally verified by diagnostic absorption bands. Complexes 1 and 3 display a pronounced broad absorption at 1384 cm^{-1} corresponding to the uncoordinated nitrate ion ($\nu_3(NO_3^-)$). Complex 2 exhibits sharp bands at 840 cm^{-1} (ν_3(P–F)) and 558 cm^{-1} (ν_4(P–F)), confirming the presence of an outer-sphere hexafluorophosphate (PF_6^-) anion. New low-frequency non-ligand bands appearing in the 480–490 cm^{-1} and 425–440 cm^{-1} regions are associated with ν(Ru–N) and ν(Ru–O)/ν(Ru–P) metal-ligand the corresponding stretching modes.[42,43] The key diagnostic FT-IR vibrational frequencies and their corresponding assignments for Complexes 1–3 are summarized in Table 3.

Table 3 Key Diagnostic FT-IR Vibrational Frequencies (cm^{-1}) and Assignments

Band Assignment	Complex 1	Complex 2	Complex 3
ν(N – H) (AMBzl amine)	3180, 3120	3210, 3145	3195, 3130
ν(C = N) (AMBzl imidazole)	1580	1585	1575
$\nu_{as}(N_3^-)$ (Azide)	2045	—	—
ν(C ≡ N) (Isothiocyanate)	—	—	2085
ν(C – S) (Isothiocyanate)	—	—	820
ν_{as}(C = O) (Oxalate)	—	1685	—
ν_s(C – O) (Oxalate)	—	1390	—
Co-ligand Modes (P – Ar / Diimine)	1098	1515	1438
pOuter-Sphere Counter Ion	1384 [$\nu_3(NO_3^-)$]	840, 558 [ν_3,$\nu_4(PF_6^-)$]	1384 [$\nu_3(NO_3^-)$]
ν(Ru – N) / ν(Ru – O/P)	485, 430	490, 440	480, 425

3.4 Electronic Absorption Spectroscopic Studies

The absorption profiles of Complexes 1–3 were acquired in 10^{-4} M DMF solution across the wavelength range of 200–800 nm at room temperature. All three complexes displayed three distinct spectral regions: high-energy intra-ligand transitions, ligand-to-metal charge transfer (LMCT) processes followed by weak d–d crystal-field transitions characteristic of low-spin d^5 Ru(III) centers in distorted octahedral geometries.[44,45]

In the ultraviolet region (240–325 nm), high-intensity absorption bands with large molar extinction coefficients ($\varepsilon > 10^4$ $M^{-1}cm^{-1}$) were observed. These bands are tentatively attributed to spin-allowed $\pi \rightarrow \pi^*$ and $n \rightarrow \pi^*$ transitions localized within the conjugated aromatic moiety of coordinated 2-aminomethylbenzimidazole (AMBzl), 5,6-dimethyl-1,10-phenanthroline (dmphen), 1,2-bis(diphenylphosphino)ethane (dppe), and triphenylphosphine (PPh_3).[46]

In the near-ultraviolet to visible range (385–480 nm), moderately intense bands were identified as LMCT transitions. For Complex 1, absorption feature at 425 nm ($\varepsilon = 3.45 \times 10^3 M^{-1}cm^{-1}$) corresponds to the $N_3(\pi) \rightarrow Ru(III)(t_{2g})$ charge transfer. Complex 2 exhibited a distinct charge transfer band centered at 410 nm ($\varepsilon = 4.15 \times 10^3 M^{-1}cm^{-1}$), originating from the $ox^{2-}(p\pi) \rightarrow Ru(III)(t_{2g})$ transition. In Complex 3, the band at 465nm ($\varepsilon = 3.80 \times 10^3 M^{-1}cm^{-1}$) is assigned to $NCS^-(\pi/\pi^*) \rightarrow Ru(III)(t_{2g})$ charge transfer.[47]

The lower-energy visible region (520 - 620 nm) was characterized by weak, broad absorption bands with low molar extinction coefficients ($\varepsilon \approx 100$ - 400 $M^{-1}cm^{-1}$). These bands are assigned to Laporte-forbidden, spin-allowed d–d crystal-field transitions ($^2T_{2g} \rightarrow {}^2A_{2g}$, $^2T_{1g}$), confirming a low-spin t_{2g}^5 (S = 1/2) electronic configuration for the central Ru(III) ion within a distorted octahedral crystal field.[48] The electronic spectral data and transition assignments for Complexes 1–3 are summarized in Table-4.

Table 4 Electronic Spectral Data and Transition Assignments in DMF (10^{-4}M)

Complex	Intra-Ligand λ_{max} (nm) [$\varepsilon \times 10^4$ $M^{-1}cm^{-1}$]	LMCT λ_{max} (nm) [$\varepsilon \times 10^3$ $M^{-1}cm^{-1}$]	d–d λ_{max} (nm) [ε $M^{-1}cm^{-1}$]	Spectral Assignments
Complex 1	255 (2.85), 295 (1.92)	425 (3.45)	545 (280)	$\pi \rightarrow \pi^*$, $N_3^-(\pi) \rightarrow Ru(III)$, $^2T_{2g} \rightarrow {}^2A_{2g}$
Complex 2	248 (3.12), 282 (2.45), 315 (1.80)	410 (4.15)	530 (320), 610 (150)	$\pi \rightarrow \pi^*$, $ox^2 \rightarrow Ru(III)$, $^2T_{2g} \rightarrow {}^2A_{2g}$, $^2T_{1g}$
Complex 3	260 (2.70), 305 (2.10)	465 (3.80)	560 (240)	$\pi \rightarrow \pi^*$, $NCS^- \rightarrow Ru(III)$, $^2T_{2g} \rightarrow {}^2A_{2g}$

3.5 Biological Evaluation, Binding Affinities, and Cytotoxic Efficacy

3.5.1 Spectroscopic Analysis of CT-DNA Binding Modes and Intrinsic Constants (K_b)

The molecular binding behavior of Complexes (1–3) to CT-DNA was evaluated by electronic absorption titration in Tris-HCl buffer (pH 7.2) according to standard procedures[33,40]. Incremental addition of CT-DNA to fixed concentrations (20 μM) of the individual Ru complex resulted in significant hypochromism (28.4 - 41.2%) with negligible bathochromic shifts (2-5 nm) at the respective charge transfer absorption bands. These spectral changes suggest the involvement of non-covalent interactions between the metal complexes and the DNA helix.[49]

The data from absorption titration was analyzed by the usual Wolfe-Shimer relation[33] to obtain the quantitative association strength. Intrinsic binding affinity constants (K_b) were derived from linear regression of the changes in the ratio of the DNA concentration to the calculated apparent extinction coefficient versus the total nucleic acid concentration. Among the complexes studied, Complex 2 showed the highest DNA binding affinity with a binding affinity constants of $4.82 \times 10^4\ M^{-1}$. The enhanced affinity may be ascribed to the planar structure of the 5,6-dimethyl-1,10-phenanthroline ligand that may undergo partial intercalation between the DNA base pairs and be further stabilized by hydrogen-bonding interactions of the amino group of the 2-aminomethylbenzimidazole moiety. The lower binding constants of complexes 1 and 3 *i.e.*, $2.15 \times 10^4\ M^{-1}$ and $1.85 \times 10^4\ M^{-1}$ in the same order indicated that such complexes bind to DNA mainly by groove binding and electrostatic interaction on the surface of DNA[50].

3.5.2 BSA Fluorescence Quenching Kinetics and Binding Site Identification (k_q, K_a)

The binding associations of Complexes 1–3 with BSA, the major transport protein for numerous drug molecules in blood plasma, were investigated by fluorescence spectroscopy. The fluorometric titrations were performed with BSA (2 μM) at an excitation wavelength of 280 nm and an emission wavelength of 346 nm, in accordance with previously reported procedures. Gradual addition of the complexes (0–30 μM) exhibited a progressive decrease with increasing concentration in the intrinsic fluorescence intensity of BSA with no appreciable change in the emission maximum.

The corresponding quenching parameters were obtained from the fluorescence quenching data by applying the Stern-Volmer equation. The calculated bimolecular quenching rate constants (k_q) for all three complexes were on the order of $10^{12}\ M^{-1}\ s^{-1}$ which significantly exceeding the diffusion-controlled limit for dynamic quenching ($2.0 \times 10^{10}\ M^{-1}\ s^{-1}$). The results indicate that the quenching mechanism is mainly of the static nature attributed to the establishment of stable ground-state associations between BSA and the Ru complexes. Moreover scatchard analysis of the binding data indicated the association constants (K_a) and indicated one predominant binding site ($n \approx 1$) in the hydrophobic Subdomain IIA (Site I) of BSA.

3.5.3 In Vitro Antiproliferative Activity against HeLa and MCF-7 Cancer Cell Lines (IC_{50})

The cytotoxic potential of Complexes (1–3) was determined by the standard colorimetric MTT assay after 48 h incubation against human cervical carcinoma (HeLa) and human breast adenocarcinoma (MCF-7) cell lines. Cisplatin was tested in parallel as a positive reference standard.

All three coordination compounds showed growth inhibition of both neoplastic lines progressively with increasing concentration. Complex 2 showed the best antiproliferative profile, with IC_{50} values of 12.4 µM against HeLa and 15.8 µM against MCF-7 cells, close to the activity of cisplatin (8.5 µM and 11.2 µM, respectively).

The pronounced cytotoxicity of the complex 2 is ascribed with its higher DNA binding constant, lipophilicity, and planar diimine ligand scaffold. The complete DNA binding constants, BSA quenching parameters, and cytotoxicity values (IC_{50}) for all complexes and cisplatin are summarized in Table 5.

Table 5 DNA Binding Constants (K_b), BSA Quenching Parameters (K_{SV}, k_q, K_a, n), and Cytotoxicity Data (IC_{50})

Biological Parameter	Complex-1	Complex-2	Complex-3	Cisplatin
CT-DNA K_b (M^{-1})	2.15×10^4	4.82×10^4	1.85×10^4	—
Hypochromism (%)	32.5	41.2	28.4	—
BSA K_{SV} (M^{-1})	1.42×10^4	2.85×10^4	1.18×10^4	—
BSA k_q (M^{-1} s^{-1})	1.42×10^{12}	2.85×10^{12}	1.18×10^{12}	—
BSA K_a (M^{-1})	3.12×10^4	5.64×10^4	2.45×10^4	—
Binding Sites (n)	0.98	1.04	0.96	—
HeLa IC_{50} (µM)	24.2 ± 1.1	12.4 ± 0.8	28.6 ± 1.4	8.5 ± 0.5
MCF-7 IC_{50} (µM)	29.8 ± 1.5	15.8 ± 0.9	34.1 ± 1.8	11.2 ± 0.6

3.6 Structure–Activity Relationship

A clear structure–activity relationship was observed among the synthesized Ru(III) complexes. Overall biological performance following the order Complex 2 > Complex 1 > Complex 3. The superior activity of Complex 2 can be primarily attributed to the presence of the planar 5,6-dimethyl-1,10-phenanthroline (dmphen) ligand. It provides an extended aromatic π-system capable of establishing favorable π–π stacking and partial intercalative interactions with DNA base pairs. The structural feature is consistent with the highest CT-DNA binding constant observed for Complex 2 (4.82×10^4 M^{-1}) compared with Complexes 1 and 3 (2.15×10^4 and 1.85×10^4 M^{-1}, respectively). The relatively planar and hydrophobic architecture of Complex 2 may also facilitate stronger hydrophobic interactions. Exhibiting protein microenvironment improve its cellular membrane permeability. This is supported by its higher BSA association constant (5.64×10^4 M^{-1}) and stronger fluorescence quenching compared with the other complexes. Complex 1 containing the flexible dppe ligand and azido co-ligands, exhibited intermediate DNA and BSA binding affinities. Whereas Complex 3 containing PPh_3 and thiocyanate ligands showed comparatively weaker biomolecular interactions. The enhanced biomolecular binding of Complex 2 is ultimately reflected in its superior antiproliferative activity with IC_{50} values of 12.4 ± 0.8 µM against HeLa and 15.8 ± 0.9 µM against MCF-7 cells. Thus the combined effects of ligand planarity, aromatic surface area, hydrophobicity, π–π interactions, biomolecular binding, and probable cellular uptake appear to play an important role in determining the biological efficacy of these Ru(III) complexes.

4 Conclusions

Three new halide-free Ru(III) complexes

containing 2-aminomethylbenzimidazole (AMBzl) were successfully synthesized and characterized using elemental analysis, molar conductivity, FT-IR, electronic absorption spectroscopy, magnetic susceptibility, and low-temperature EPR measurements. The physicochemical and spectroscopic results support the formation of mononuclear, low-spin Ru(III) complexes with distorted octahedral coordination environments and 1:1 electrolytic behavior, with nitrate (NO_3^-) and hexafluorophosphate (PF_6^-) present as outer-sphere counter ions. The combined spectroscopic and magnetic data further confirmed the coordination of AMBzl and the respective pseudohalide, oxalate, phosphine, and diimine ligands around the Ru(III) center. The biological studies demonstrated that modification of the ancillary ligand environment substantially influences the biomolecular interactions and antiproliferative activity of the complexes. Overall the present study demonstrates that halide-free Ru(III)–benzimidazole complexes provide a tunable platform for the development of biologically active Ru-based metallodrug candidates and warrants further investigation of their cellular mechanisms in vivo therapeutic potential.

5 Scope for Future Research

The present study has shown the promising DNA binding ability, protein interaction properties and anticancer activity of the synthesized Ru(III) complexes. But more work is needed to explore their full therapeutic potential. Future studies may be aimed to understand the detailed mechanism of interaction of such complexes with cellular targets and how they induce cancer cell death. Testing of these compounds in other cancer cell lines and drug resistant tumor models may provide a broader perspective on their biological activity.

Further work should include toxicity studies on normal cells to define selectivity and safety. In vivo studies on animal models suitable for the evaluation of the pharmacokinetic behavior, biodistribution and therapeutic efficacy under physiological conditions will be useful. In addition, the structural modification of the ligand system may contribute to the development of new ruthenium complexes with enhanced biological activity and better medicinal properties. These studies may open the way to the development of effective ruthenium-based metallodrugs in the future.

6 Acknowledgements

The authors are thankful to the Department of Chemistry, Tilka Manjhi Bhagalpur University, Bhagalpur, for providing the necessary laboratory facility and administrative support for carrying out the research work. We also thank the Department of Chemistry, College of Commerce, Arts & Science, Patna (Patliputra University) for collaborative support. We thank the Sophisticated Analytical Instrument Facility (SAIF) at IIT Patna for instrumental analyses, which are crucial to the structural elucidation of the complexes.

MANUSCRIPT DECLARATIONS & STATEMENTS

Conflict of Interest: The authors declare that they have no competing financial interests or personal relationships that could have appeared to influence the work reported in this manuscript.

Funding Statement: The authors received no specific financial support for this work from any public, commercial, or not-for-profit funding agencies.

References

1. Zeng, L.; Gupta, P.; Chen, Y.; Wang, E.; Ji, L.;

Chao, H.; Chen, Z.-S. *Chem. Soc. Rev.*, 2017, *46*, 5771–5804. DOI: https://doi.org/10.1039/c7cs00195a

2. Lee, S. Y.; Kim, C. Y.; Nam, T.-G. *Drug Des. Devel. Ther.*, 2020, *14*, 5375–5392. DOI: https://doi.org/10.2147/DDDT.S275007
3. Sun, Q.; Li, Y.; Shi, H.; Wang, Y.; Zhang, J.; Zhang, Q. *Molecules*, 2021, *26*, 4389. DOI: https://doi.org/10.3390/molecules26154389
4. D'Amato, A.; Mariconda, A.; Iacopetta, D.; Ceramella, J.; Catalano, A.; Sinicropi, M. S.; Longo, P. *Pharmaceuticals*, *2023*, *16*, 1729. DOI: https://doi.org/10.3390/ph16121729
5. Alessio, E. *Eur. J. Inorg. Chem.*, *2017*, 2017, 1549–1560. DOI: 10.1002/ejic.201600986
6. Khan, R. A.; AlFawaz, A.; Farshori, N. N.; Paul, A.; Jaafar, M. H.; Alsalme, A. *Appl. Organomet. Chem.*, 2022, *36*, e6702. DOI: https://doi.org/10.1002/aoc.6702
7. Rogala, P.; Jabłońska-Wawrzycka, A.; Czerwonka, G.; Kazimierczuk, K.; Gałczyńska, K.; Michałkiewicz, S.; Kalinowska Tłuścik, J.; Karpiel, M.; Klika, K. D. *Molecules*, 2023, *28*, 40. DOI: https://doi.org/10.3390/molecules28010040
8. Chakraborty, A.; Roy, S.; Chakraborty, M. P.; Saha Roy, S.; Purkait, K.; Koley, T. S.; Das, R.; Acharya, M.; Mukherjee, A. *Inorg. Chem.*, 2021, *60*, 18379–18394. DOI: https://doi.org/10.1021/acs.inorgchem.1c02979
9. Welsh, A.; Rylands, L.-I.; Arion, V. B.; Prince, S.; Smith, G. S. *Dalton Trans.*, 2020, *49*, 1143–1156. DOI: 10.1039/C9DT03902C
10. Kanchanadevi, S.; Fronczek, F. R.; Mahalingam, V. *Inorg. Chim. Acta*, *2021*, *526*, 120532. DOI: https://doi.org/10.1016/j.ica.2021.120532
11. Zhang, Z.; Yang, Z.; Wu, Y.; Yuan, Z.; Du, J.; Li, L. *J. Biochem. Mol. Toxicol.*, *2020*, *34*, e22510. DOI: https://doi.org/10.1002/jbt.22510
12. Maikoo, S.; Chakraborty, A.; Vukea, N.; Kirkpatrick Dingle, L. M.; Samson, W. J.; de la Mare, J.; Edkins, A. L.; Booysen, I. N. *J. Biomol. Struct. Dyn.*, *2021*, *39*, 4077–4088. DOI:https://doi.org/10.1080/07391102.2020.1775126
13. Oliveira, K. M.; Honorato, J.; Gonçalves, G. R.; Cominetti, M. R.; Batista, A. A.; Correa, R. S. *Dalton Trans.*, *2020*, *49*, 12643–12652. DOI: https://doi.org/10.1039/d0dt01591a
14. Das, A.; Mandal, S.; Mukherjee, R.; Naskar, R.; Murmu, N.; Mondal, T. K. *New J. Chem.*, *2023*, *47*, 17359–17372. DOI: https://doi.org/10.1039/d3nj02391e
15. Sayala, J.; Srivastava, E.; Kumar, P.; Shukla, N.; Kumar, A.; Patra, A. K. *Dalton Trans.*, *2024*, *53*, 4580–4597. DOI: https://doi.org/10.1039/d3dt04058e
16. Tsaulwayo, N.; Omondi, R. O.; Vijayan, P.; Sibuyi, N. R. S.; Meyer, M. D.; Meyer, M.; Ojwach, S. O. *RSC Adv.*, *2024*, *14*, 8322–8330. DOI: https://doi.org/10.1039/d4ra00525b
17. Sindhu, M.; Kalaivani, P.; Prabusankar, G.; Sivasamy, R.; Prabhakaran, R. *Dalton Trans.*, *2024*, *53*, 3075–3096. DOI: https://doi.org/10.1039/d3dt04017h
18. Opaèak, S.; Pernar Kovaè, M.; Brozovic, A.; Piantanida, I.; Kirin, S. I. *Dalton Trans.*, *2023*, *52*, 11698–11704. DOI: https://doi.org/10.1039/d3dt02289g
19. Zahiroviæ, A.; Roca, S.; Kahroviæ, E.; Višnjevac, A. *J. Mol. Struct.*, *2021*, *1236*, 130326. DOI: https://doi.org/10.17344/acsi.2022.7826
20. Candido, C. C.; Silva, H. V. R.; Zavan, B.; Ionta, M.; Barbosa, M. I. F.; Doriguetto, A. C. *J. Inorg. Biochem.*, *2022*, *237*, 112022. DOI: https://doi.org/10.1016/j.jinorgbio.2022.112022
21. Teixeira, T.; Ribeiro, G. H.; Gonçalves, G. R.; Honorato, J.; Oliveira, K. M.; Correa, R. S. *Inorg. Chim. Acta*, *2024*, *568*, 122078. DOI: https://doi.org/10.1016/j.ica.2024.122078
22. Pathan, J.; Tripathi, D. K.; Poluri, K. M.; Chalana, A.; Adhikari, S. *J. Inorg. Biochem.*, *2024*, *257*, 112584. DOI: https://doi.org/10.1016/j.jinorgbio.2024.112584
23. Bibi, R.; Zahid, M.; Rasool, F.; Tariq, M.;

Hussain, A.; Asif, H. M.; Khan, M. A.; Shah, K. H.; Hussain, S.; Sirajuddin, M.; Yar, M.; Ayub, K. *Spectrochim. Acta A Mol. Biomol. Spectrosc.*, *2025*, *330*, 125630. DOI: https://doi.org/10.1016/j.saa.2024.125630

24. Badr, H. E.; Elsayed, S. A.; Kawde, A.-N.; El-Hendawy, A. M. *Inorg. Chem. Commun.*, *2025*, *181*, 115287. DOI: https://doi.org/10.1016/j.inoche.2025.115287
25. Joshi, B.; Shivashankar, M. *Inorg. Chem. Commun.*, *2025*, *180*, 115038. DOI: https://doi.org/10.1016/j.inoche.2025.115038
26. Kavukcu, S. B.; Vatansever, H. S.; Ilhan, S.; Türkmen, H. *Bioinorg. Chem. Appl.*, *2025*, *2025*, 5556956. DOI: https://doi.org/10.1155/bca/5556956
27. Eswaran, J.; Mariappan, A.; Arumugham, N.; Murugan, T.; Bhuvanesh, N. S. P.; Anathakrishnan, N. M.; Daniel, S.; Kanthapazham, R. *J. Mol. Struct.*, *2022*, *1270*, 133929. DOI: https://doi.org/10.1016/j.molstruc.2022.133929 0022-2860
28. Neethu, K. S.; Eswaran, J.; Murugan, T.; Bhuvanesh, N. S. P.; Neelakantan, M. A.; Velusamy, K. M. *Appl. Organomet. Chem.*, *2019*, *33*, e4751. DOI: https://doi.org/10.1002/aoc.4751
29. Gramni, L.; Vukea, N.; Chakraborty, A.; Samson, W. J.; Kirkpatrick Dingle, L. M.; Xulu, B.; de la Mare, J. A.; Edkins, A. L.; Booysen, I. N. *Inorg. Chim. Acta*, *2019*, *492*, 98–107. DOI: https://doi.org/10.1016/j.ica.2019.04.018
30. Manjuraj, T.; Prashanth Kumar, P. N.; Vasantha Kumar, B. C.; Imadadulla, M.; Shivarudrappa, H. P.; Desai, S. M.; Lokesh, M. R. *Asian J. Chem.*, *2025*, *37*, 2265–2273. DOI: https://doi.org/10.14233/ajchem.2025.34233
31. Namani, M.; Nambigari, N. *Asian J. Chem.*, *2026*, *38*, 1862–1872. DOI: https://doi.org/10.14233/ajchem.2026.36068
32. Kalita, R. M.; Baruah, R. S.; Medhi, C. *Asian J. Chem.*, *2021*, *33*, 859–866. DOI: https://doi.org/10.14233/ajchem.2021.23099
33. Devi, R. S.; Kumaraguru, N. *Asian J. Chem.*, *2020*, *32*, 665–677. DOI: https://doi.org/10.14233/ajchem.2020.22485
34. Devi, R. S.; Kumaraguru, N. *Asian J. Chem.*, *2019*, *31*, 1931–1942. DOI: https://doi.org/10.14233/ajchem.2019.21990
35. Kaushal, R.; Kaur, M.; Sheetal; Sharma, J.; Nehra, K. *J. Mol. Struct.*, *2024*, *1295*, 136788. DOI: https://doi.org/10.1016/j.molstruc.2023.136788
36. Mathuba, Y. W.; Makuve, N.; Manyepedza, T. *Orient. J. Chem.*, *2025*, *41*, 1733–1748. DOI: https://doi.org/10.13005/ojc/410615
37. Bharate, Y. N.; Sakhare, M. A.; Jadhav, S. B.; Naikwade, S. D. *Rasayan J. Chem.*, *2021*, *14*, 479–485. DOI: http://dx.doi.org/10.31788/RJC.2021.1416097
38. Msimango, N.; Welsh, A.; Prince, S.; Smith, G. S. *Inorg. Chem. Commun.*, *2022*, *144*, 109840. DOI: https://doi.org/10.1016/j.inoche.2022.109840
39. Dömötör, O.; Teixeira, R. G.; Spengler, G.; Avecilla, F.; Marques, F.; Lenis-Rojas, O. A.; Matos, C. P.; de Almeida, R. F. M.; Enyedy, É. A.; Tomaz, A. I. *J. Inorg. Biochem.*, *2023*, *238*, 112058. DOI: https://doi.org/10.1016/j.jinorgbio.2022.112058
40. Hu, X.; Luo, Q.; Qin, Y.; Wu, Y.; Liu, X.-W. *Molecules*, *2022*, *27*, 3676. DOI: https://doi.org/10.3390/molecules27123676
41. dos Santos, E. R.; Graminha, A. E.; Schultz, M. S.; Correia, I.; Selistre-de-Araújo, H. S.; Corrêa, R. S.; Ellena, J.; Lacerda, E. P. S.; Pessoa, J. C.; Batista, A. A. *J. Inorg. Biochem.*, *2018*, *182*, 48–60. DOI: https://doi.org/10.1016/j.jinorgbio.2017.12.010
42. da Silva, E. N.; da Silva, P. A. B.; Graminha, A. E.; de Oliveira, P. F.; Damasceno, J. L.; Tavares, D. C.; Batista, A. A.; Von Poelhsitz, G. *Bioinorg. Chem. Appl.*, *2017*, *2017*, 2562780. DOI: https://doi.org/10.1155/2017/2562780
43. Poynton, F. E.; Bright, S. A.; Blasco, S.;

Williams, D. C.; Kelly, J. M.; Gunnlaugsson, T. *Chem. Soc. Rev.*, *2017*, *46*, 7706–7756. DOI: https://doi.org/10.1039/C7CS00680B

44. Jayanthi, E.; Venkataramana, M.; Sankar, N.; Bhuvanesh, N. S. P.; Dharmaraj, N. *Polyhedron, 2017*, *132*, 39–52. DOI: https://doi.org/10.1016/j.poly.2017.04.026
45. Jacinto, F. E.; de Oliveira, L. P.; Batista, A. A.; Oliveira, K. M.; Correa, R. S. *R. Soc. Open Sci.*, *2024*, *11*, 240353. DOI: https://doi.org/10.1098/rsos.240353
46. Gobbo, A.; Vanèo, J.; Benetti, S.; Malina, T.; Dvoř ák, Z.; Castelli, C.; Chiappa, A.; Guelfi, M.; Zacchini, S.; Biver, T.; Trávníèek, Z.; Marchetti, F. *Inorg. Chem.*, *2025*, *64*, 24615–24633. DOI: https://doi.org/10.1021/acs.inorgchem.5c04198 2318. DOI: HTTPS://DOI.ORG/
47. Bibi, R.; Fatima,S.; Sadiq, J. ; Tariq, M.; Hussain, A.;Rasool, F.; Iqbal, S.; Shah, K.H.; Hussain,S.; Sirajuddin, M. ; Yar,M. ; Ayub, K.J.; Oraganoment. Chem.,2025,1038,123775. DOI: https://doi.org/10.1016/j.jorganchem.2025.123775.
48. Singh, K.; Kumari, B.; Sharma, A. Rasayan J. Chem., 2021, 14, 29-35. DOI: https://doi.org/10.31788/RJC.2021.1416108
49. Karthikeyan, G.; Kalaivani, P.; Prabusankar, G.; Sivasamy, R.; Prabhakaran, R. Molecules, 2020, 25, 4284. DOI: https://doi.org/10.3390/molecules25184284
50. Singh, A. K.; Katheria, S.; Kumar, A.; Zafri, A.; Arshad, M. Asian J. Chem., 2019,31,2311-2318. DOi: https://doi.org/10.14233/ajchem.2019.22162